RESEARCH ARTICLE

WILEY

Carboxylated carbon nanotubes with high electrocatalytic activity for oxygen evolution in acidic conditions

Xin Zhang[1] | Wenqing Zhang[1] | Jianying Dai[1] | Mingzi Sun[2] | Jun Zhao[1] |
Lifei Ji[1] | Lin Chen[1] | Fanlong Zeng[1] | Fengchun Yang[1] (ORCID) |
Bolong Huang[2] | Liming Dai[3]

[1]Key Laboratory of Synthetic and Natural Functional Molecule Chemistry (Ministry of Education), College of Chemistry and Material Science, Northwest University, Xi'an, China

[2]Department of Applied Biology and Chemical Technology, The Hong Kong Polytechnic University, Kowloon, Hong Kong SAR, China

[3]Centre of Advanced Carbon Materials, School of Chemical Engineering, University of New South Wales, Sydney, Australia

Correspondence
Fengchun Yang, Key Laboratory of Synthetic and Natural Functional Molecule Chemistry (Ministry of Education), College of Chemistry and Material Science, Northwest University, Xi'an, China.
Email: fyang@nwu.edu.cn

Bolong Huang, Department of Applied Biology and Chemical Technology, The Hong Kong Polytechnic University, Hung Hom, Kowloon, Hong Kong SAR, China.
Email: bhuang@polyu.edu.hk

Liming Dai, Centre of Advanced Carbon Materials, School of Chemical Engineering, University of New South Wales, Sydney, Australia.
Email: l.dai@unsw.edu.au

Abstract

Since most electrocatalysts for oxygen evolution reaction (OER), except for precious metal oxides RuO_2 and IrO_2, are unstable in harsh acidic solutions, it is highly desirable to develop high-performance OER electrocatalysts for acidic media, though it is still a big challenge. Herein, we report a simple strategy to produce carboxyl-enriched multiwalled carbon nanotubes (COOH-MWNTs) that exhibit stable and high electrocatalytic activities for OER in acidic solutions, showing an overpotential at a current density of 10 mA cm^{-2} and a Tafel slope as low as of 265 mV and 82 mV dec^{-1}, respectively. As far as we are aware, these results represent the best OER performance for metal-free electrocatalysts, even comparable to those of RuO_2 and IrO_2. We have further revealed the catalytic mechanism, which involves one electron lose from the COOH-MWNTs catalyst at the beginning of the OER process to trigger H_2O molecule oxidation by forming peralcohol, followed by the recapture of one electron from water molecule to oxidize water and to recover the initial state for the COOH-MWNTs catalyst. The unravel of this new OER mechanism is important as it provides new insights into the crucial role of organic functional groups in electrocatalytic processes. Also, the mechanistic understanding can be used to guide the design and development of novel metal-free catalysts for acidic OER electrocatalysis and beyond.

KEYWORDS
acidic oxygen evolution, carbon nanotubes, carboxylation defect, metal-free, catalytic mechanism

Xin Zhang and Wenqing Zhang contributed equally to this study.

1 | INTRODUCTION

The oxygen evolution reaction (OER) is a critical half reaction in water splitting and metal-air batteries.[1,2] Performing the OER in acidic media has practical significance due to the high mass transfer rate, product purity and good efficiency for the acidic electrocatalysis.[3,4] Unfortunately, the vast majority of OER electrocatalysts with excellent catalytic performance in alkaline media are unstable in harsh acidic solutions.[5,6] So far, precious metal Ruthenium (Ru) and iridium (Ir) oxides have emerged as the best two OER catalysts in acidic media.[7,8] However, the limited availability and high cost of these noble metals have severely limited their large-scale applications. Therefore, it is important to develop efficient, stable, and low-cost OER catalyst for electrocatalysis in acidic media, though still a significant challenge.[9]

Recently, metal-free catalysts based on carbon nanotubes (CNTs), such as heteroatom-doped, charge-adsorbed and defective CNTs, have been demonstrated to show great potential for enhancing electrocatalysis in alkaline media through charge/spin redistribution.[10–14] However, these catalysts generally display severely degraded OER properties in acids (Figure S1) owing to their inherent strong hydrophobicity in acidic conditions (Figure S2) to block the contact between the catalyst and H_2O molecules. This limitation could be overcome by introducing appropriate oxygen-containing groups, such as hydroxyl, epoxy and carboxyl moieties, on the CNTs surface to enhance their hydrophilicity.[15] Compared with carboxyl, the hydroxyl and epoxy groups are unstable and are subjected to further oxidization in the OER process, especially in acidic conditions.[16] Thus, the incorporation of carboxyl groups is an attractive option to guarantee both the hydrophilicity and electrocatalytic stability of CNTs, even in acidic media. Moreover, the strongly electron-withdrawing carboxyl group can reduce the local electronic density of CNTs, which, for an oxidation reaction (i.e., OER), could facilitate charge transfer from solution to the CNTs electrode to accelerate the water oxidation process.[17] Therefore, carboxylation of CNTs appears as a desirable route to enhance their OER performance under acidic conditions, leading to a new class of metal-free carbon electrocatalysts by covalent functionalization of carbon nanomaterials even without heteroatom-doping – a great potential that has not been previously recognized, though certain functionalized carbon catalysts have long been used for some non-electrochemical reactions or simple electrochemical reaction (e.g., oxygen reduction) without mechanistic understanding.[18,19]

Herein, we report a facile hydrothermal acid oxidation of CNTs to produce carboxyl-enriched multiple-walled carbon nanotubes (COOH-MWNTs), which exhibited unprecedented OER performance in acidic conditions with a low overpotential of 265 mV at a current density of 10 mA cm^{-2} and a small Tafel slope of 82 mV dec^{-1}—better OER performance than that of any metal-free electrocatalysts in acidic conditions reported to date[20–25] and comparable to those of the RuO_2 and IrO_2 benchmark catalysts. Our experimental observations combined with the theoretical calculations revealed a novel OER mechanism for the carboxyl-enriched MWNTs catalysts, in which the carboxyl group lowers the energy barrier for water splitting via the formation and hydrolysis of a lactone. The observed excellent catalytic performance and demonstrated unique catalytic mechanism clearly indicate the feasibility to use the simple strategy presented in this paper for developing novel carbon-based metal-free catalysts with improved electrocatalytic activity in acidic media, attractive for high-performance water splitting, metal-air batteries and beyond.

2 | RESULTS AND DISCUSSION

Carboxyl-enriched MWNTs with different oxygen contents (Figure S3 and Table S1) were prepared by oxidation of MWNTs (see Figure S4 for the possible structure) in piranha solution for different times (10–30 h), followed by subsequent hydrothermal treatment in oxygen-saturated solution. The MWNTs in the resultant COOH-MWNTs maintained an intact tubular structure (Figures 1A and S5), but their surface hydrophilicity increased significantly in respect to their pristine counterparts in 0.5 M H_2SO_4, as shown in the insets of Figure 1A and in Figure S6. These effects favor the COOH-MWNTs for efficient electrocatalysis in acid electrolytes. However, an increase in the carboxyl content could cause an inevitable damage of the MWNTs structure, and a concomitant decrease in its electrical conductivity (Figures 1B and S7), leading to a poor electrocatalytic activity. As shown in the inset of Figures 1B and S8, the as-prepared COOH-MWNTs with an oxygen content of about 3.9 at% showed the lowest onset potential in acidic conditions among all the samples investigated in this study, with a balanced hydrophilicity and electrical conductivity. Thus, this particular sample obtained after 20 h oxidation and hydrothermal treatment (denoted as: COOH-3.9-MWNTs) was used for subsequent analyses, along with the precursor MWNTs (by oxidation for 20 h but without subsequent hydrothermal treatment, denoted as: o-MWNTs) for comparison.

Figure 1C shows the high-resolution O 1s XPS spectra of COOH-3.9-MWNTs and o-MWNTs samples. As can be seen, the MWNTs were successfully oxidized to show the
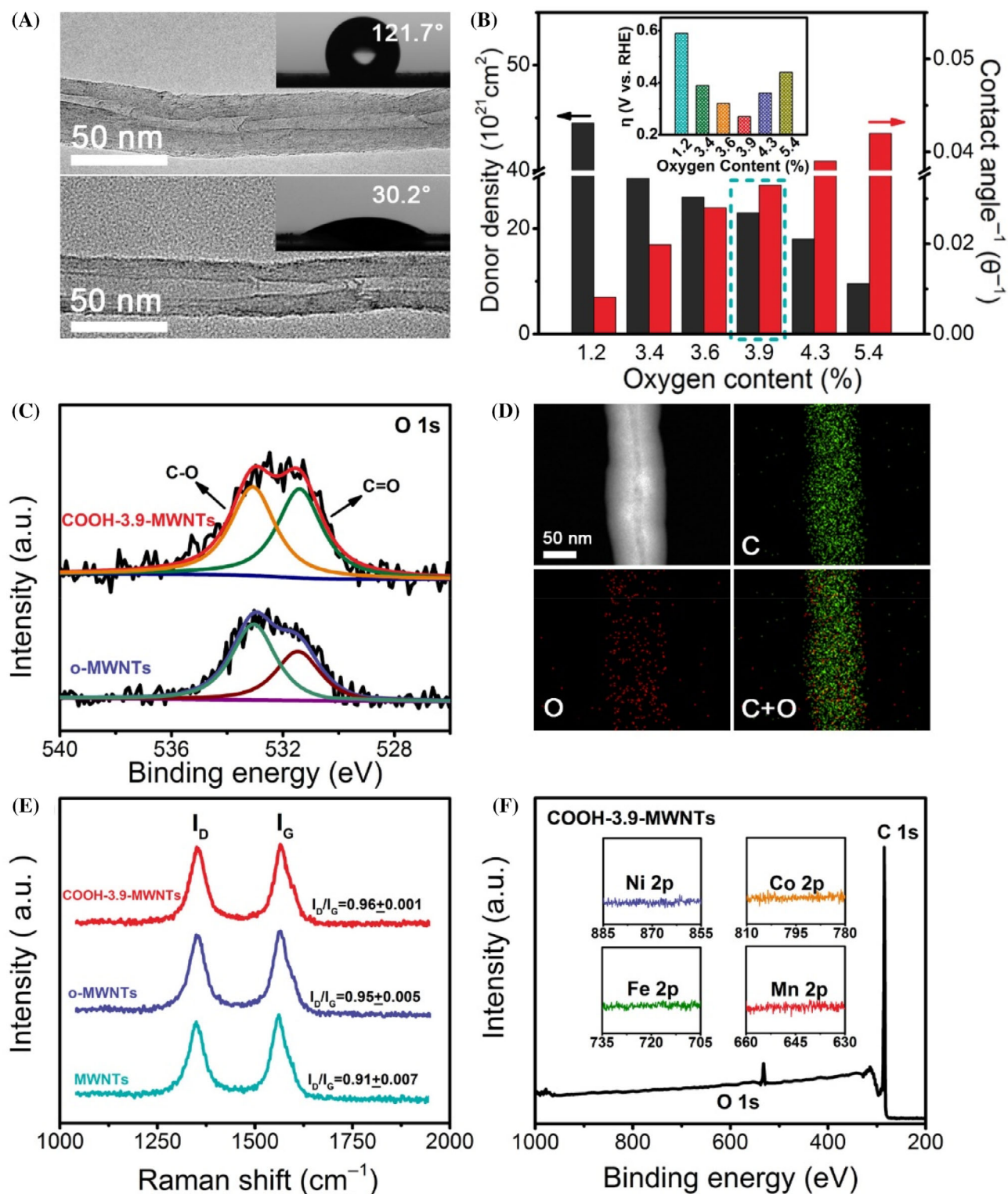
FIGURE 1 (A) TEM images of corresponding water contact angles in 0.5 M H₂SO₄ (insets) of pristine and COOH-MWNTs. (B) Contact angle, donor density, and overpotential of carboxylic MWNTs with different oxygen contents. (C) O 1s XPS spectra of COOH-3.9-MWNTs and o-MWNTs samples. (D) EDS elemental mapping images showing C (green) and O (red) distributions in COOH-3.9-MWNTs sample. (E) Raman spectra of COOH-3.9-MWNTs, o-MWNTs, and pristine MWNTs samples. (F) XPS survey spectrum of COOH-3.9-MWNTs; the insets show the Ni 2p, Co 2p, Fe 2p, and Mn 2p spectra

presence of the C—O and C=O peaks with an intensity ration (I(C—O)/I(C=O)) of approximately 2:1 for o-MWNTs, arising from the oxygen-containing groups, such as hydroxyl, epoxy, and carboxyl groups, in the oxidized MWNTs. After the hydrothermal treatment in oxygen-saturated solution, the content of ketonic C=O groups increased, and the I(C—O)/I(C=O) decreased to 1:1; suggesting that carboxyl groups became dominant in the COOH-MWNTs, as also confirmed by Fourier transform infrared spectroscopy (FT-IR, Figure S9).[26] The energy dispersive spectroscopy (EDS) mappings in Figure 1D show a homogeneous distribution of oxygen atoms in the COOH-3.9-MWNTs, confirming that the carboxyl groups are evenly spread over the nanotubes. Raman spectra in Figure 1E show an increased number of defects in o-MWNTs compared with the MWNTs, whereas the defect content in COOH-MWNTs shows only a minimal change with respect to that of o-MWNTs. Both the XPS and Raman results indicate that the hydrothermal treatment caused the transformation of hydroxyl or epoxy into carboxyl groups, rather than introducing new defects. Furthermore, only the C and O peaks, but no peak for metal (Ni, Co, Fe, Mn) impurities, could be detected in the XPS survey spectrum of COOH-3.9-MWNTs (Figure 1F), and its metal content was found to be as low as 0.01 wt % by inductively coupled plasma-atomic emission spectrometry (ICP-AES, Table S2). Therefore, this carboxyl-enriched MWNTs sample represents a suitable model catalyst for further analysis in this study, due to the predominant content of carboxyl groups (with a key role in the OER process) and the negligible effect of defects or metal impurities.

The OER performance of the COOH-3.9-MWNTs was evaluated in 0.5 M H_2SO_4 using a three-electrode cell with a loading of 1.41 mg cm^{-2} (Figure S10). As shown by the linear sweep voltammetry (LSV) curves in Figure 2A and S11, the optimized COOH-3.9-MWNTs sample displayed outstanding OER performance in the acid electrolyte with a small overpotential of 265 mV at 10 mA cm^{-2}, much lower than that of o-MWNTs (420 mV) and commercial RuO_2 (310 mV). As seen in Figures 2B and S12, the COOH-3.9-MWNTs also showed a similar Tafel slope and a higher exchange current density (82 mV dec^{-1} and 9.3 μA cm^{-2}, respectively) compared to those of RuO_2 (66 mV dec^{-1} and 0.61 μA cm^{-2}, respectively). Also, the COOH-3.9-MWNTs maintained a high OER activity in 0.1 M $HClO_4$ with a small η10 of 290 mV and a Tafel slope of 103 mV dec^{-1} (Figure S13). These results highlight the fast kinetics for the COOH-3.9-MWNTs, as also reflected by its small charge transfer resistance measured with electrochemical impedance spectroscopy (EIS, Figure S14) and its high electrochemically active surface area (ECSA, Figures 2C and S15). Although the defect contents of COOH-

3.9-MWNTs and o-MWNTs were almost the same (Figure 1E), the ECSA of COOH-3.9-MWNTs was nearly 2.5 times higher than that of o-MWNTs. These results indicate that the increase in ECSA could be attributed to the presence of carboxyl groups,[27] which rendered the CNTs surface hydrophilic (Figures 1A and S6) to enhance its interaction with the electrolyte and charge-transfer to the reactant (*vide infra*), and hence the facilitated OER at the COOH-3.9-MWNTs catalyst. We further performed SCN$^-$ poisoning tests and found no change in the OER performance of COOH-3.9-MWNTs before and after the addition of KSCN. In contrast, a severe decrease in current density was observed for MWNTs supported on metallic Ni (Figure 2D). Clearly, therefore, the effect of residual metal impurities on the OER activity, if any, was negligible for COOH-3.9-MWNTs.

Figure 2E shows that the polarization curves of COOH-3.9-MWNTs before and after 3000 sweep cycles exhibited no visible change, with only a 6% current loss after 10 h of the chronoamperometric testing (inset of Figure 2E). In contrast, the commercial RuO_2 was quite unstable under the same conditions (Figure S16). The scanning electron microscopy (SEM) images in Figure S17 show that the COOH-3.9-MWNTs retained their tubular structure after the durability test. Besides, the C=O and C—O peaks in the O 1s XPS spectrum did not change after the stability testing (Figures S18 and 1C), demonstrating, once again, the excellent electrocatalytic stability of COOH-3.9-MWNTs in acidic media. As shown in Figure S19, no CO_2 was detected by gas chromatography after the OER process, suggesting no degradation of carbon nanotubes even under the strong acidic conditions. Overall, the above durability tests highlight an excellent stability of the carboxyl-enriched MWNTs, including the carboxyl groups.

The gas evolution from COOH-3.9-MWNTs was further investigated using a rotating ring disk electrode (RRDE) in 0.5 M H_2SO_4 (Figure 2F). It was demonstrated that the oxygen reduction reaction (ORR) occurred on the Pt ring electrode as soon as the oxidative current increased at the disk electrode, indicating an immediate and intensive oxygen generation catalyzed by COOH-3.9-MWNTs under the appropriate overpotential (Figures 2F and S20). On the other hand, a weak ORR current was obtained for the o-MWNTs, denoting a highly inefficient OER process for the o-MWNTs (Figure S21). The Faradaic efficiency of COOH-3.9-MWNTs reached 98% when the disk current was held at 270 μA (Figure S22).[28] Meanwhile, the yield of O_2 via OER is approximate to the production in theoretically, indicating the Faradaic efficiency is approach to 100% (Figure S23). In addition, no H_2O_2 was detected by the ring electrode during the OER process (Figure S24), indicating that oxygen evolution from the
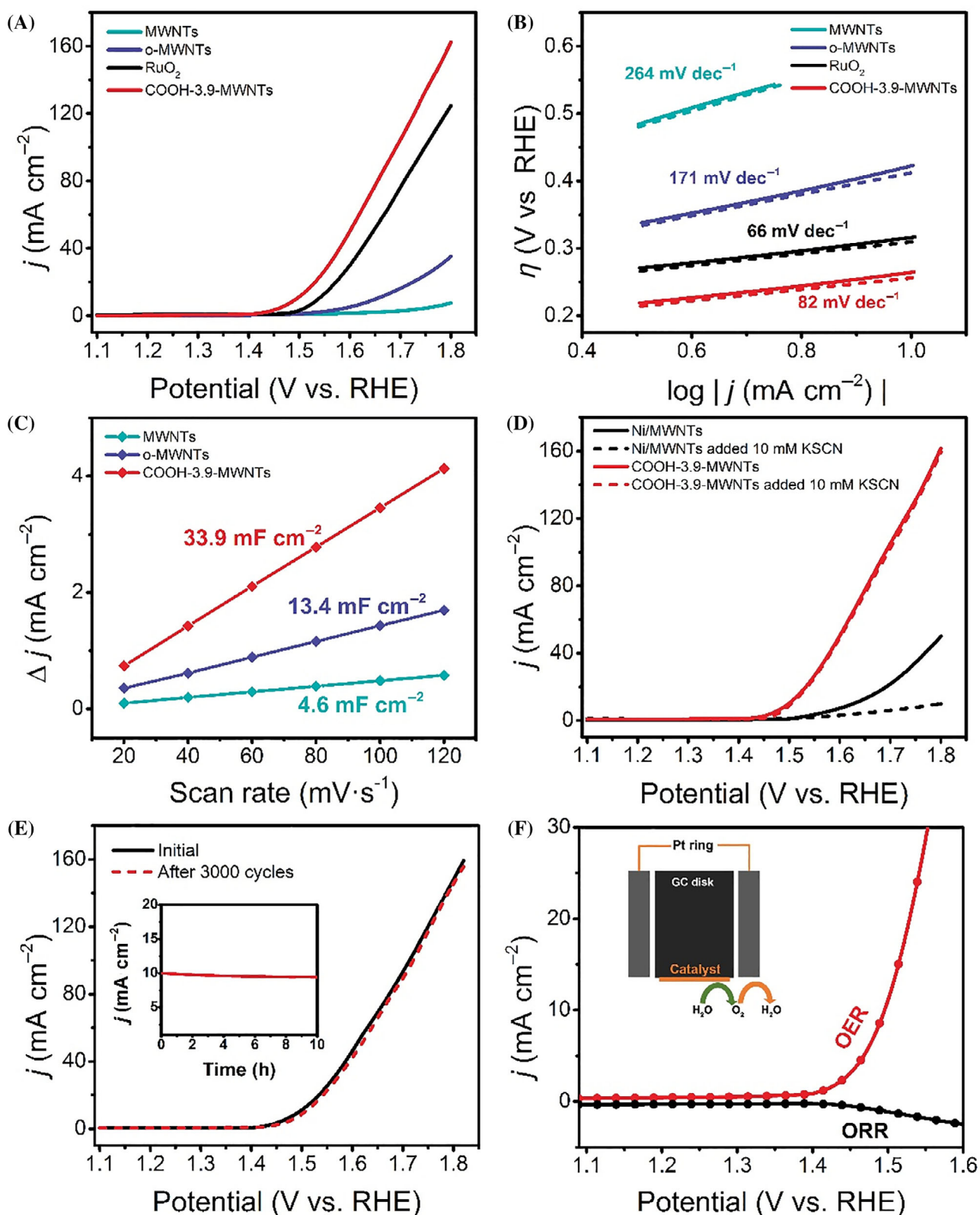
FIGURE 2 (A) LSV curves and (B) corresponding Tafel plots for the OER of COOH-3.9-MWNTs, o-MWNTs, MWNTs, and commercial RuO_2 in 0.5 M H_2SO_4. (C) Anodic capacitance current plots. (D) OER activity of COOH-3.9-MWNTs and Ni/MWNTs samples before and after addition of 10 mM KSCN in 0.5 M H_2SO_4. (E) Stability test of COOH-3.9-MWNTs in 0.5 M H_2SO_4. (F) O_2 evolution from the COOH-3.9-MWNTs during the OER process, detected using a rotating ring disk electrode at a constant potential of 0.4 V versus RHE

COOH-3.9-MWNTs involved a fast four-electron transfer process.[29]

The above results indicate that the remarkable OER performance of the COOH-3.9-MWNTs in an acidic OER is attributable to the carboxyl surface groups on the nanotubes. However, the mechanistic understanding of how the MWNTs-supported carboxyl groups can catalyze the OER process is unclear. Based on the theoretical and experimental results to be discussed below, we propose a plausible mechanism for the OER process catalyzed by the carboxyl-functionalized MWNTs in acidic media. As shown in Scheme 1, the anodic oxidization of the defective carbon atom adjacent to the carboxylic group in **1** gives the active species **2**. Then, annulation of **2** driven by electrostatic interactions produces the lactone **3**. Hydrolyzation of **3** yields the key intermediate **4** via water splitting, and subsequent anodic oxidation transforms **4** to peroxide **6** through epoxide **5**. Finally, the tertiary radical in **6** could induce homogenous cleavage of the vicinal peroxide functionality to release molecular oxygen along with a proton and an electron and regenerate neutral aromatic carboxylic acid **1** for next catalytic cycle. Unlike metal-based catalysts that have high capabilities to rapidly capture electrons from water molecules, the carboxyl-enriched carbon nanotubes must use their own electrons to trigger the formation and hydrolysis of a lactone and recapture their electrons at the end of the cycle, recovering the initial state (Scheme 1).

The above catalytic mechanism was supported by our theoretical calculations and experimental observations. In particular, we calculated the reactivity of CNTs containing different functional groups, including CNTs with vacancies (Figure 3A), CNTs with —COOH groups (i.e., COOH-MWNTs), and the key intermediate **3** (Scheme 1, Figure 3B). As seen in Scheme 1, the structure of intermediate **4** and the formation of O_2 (Figure 3C,D) confirm that the active sites of the CNTs are the carboxyl groups introduced at defect sites. Figure 3E gives the projected partial density of states (PDOS) plots, which shows that the O 2p orbitals are shifted to higher energies by bonding unsaturation, where the electron pair results in a stronger tendency for oxidation. The main contribution to the activity of the lactone **3** comes from the p-π divalent [C=O] bonds, whose O 2p states are closer to the Fermi level (E_F) than those of the nearby [—O—C—O—] bonds with higher electron density, suggesting a higher reactivity. The electrons originating from the two oxygen atoms bonded with edge carbon atoms could produce a local electron-rich environment, causing strong adsorption of water molecules and enhancing the OER
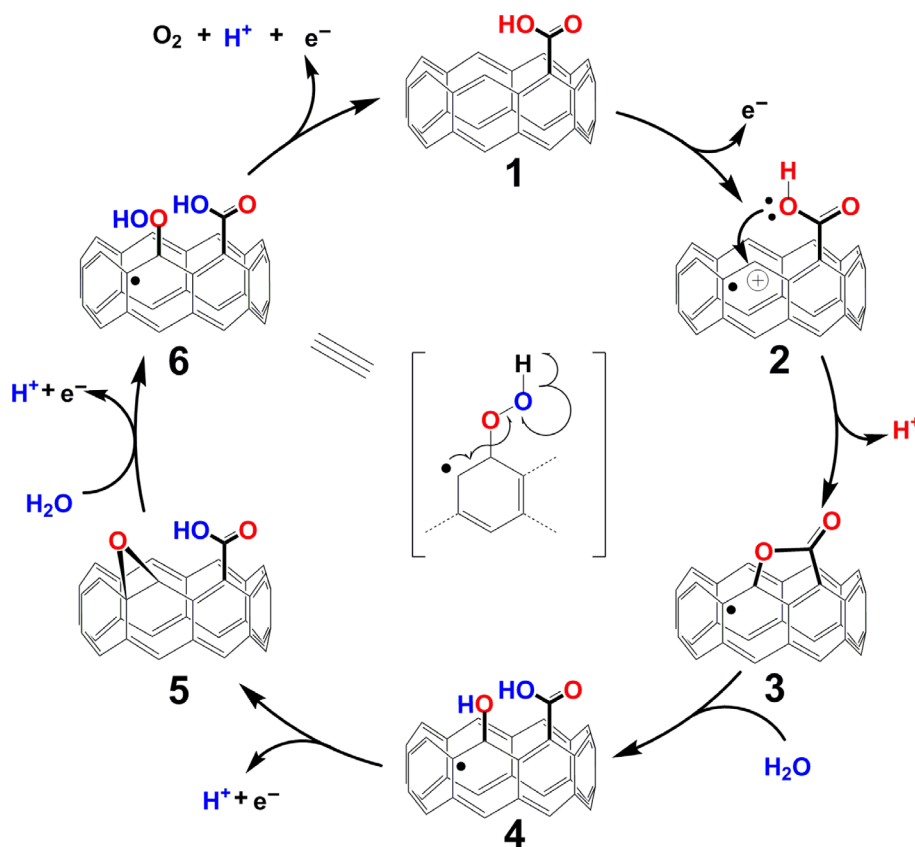
SCHEME 1 Possible mechanism for water oxidation on carbon atoms adjacent to carboxylic acid groups in COOHs-MWNTs
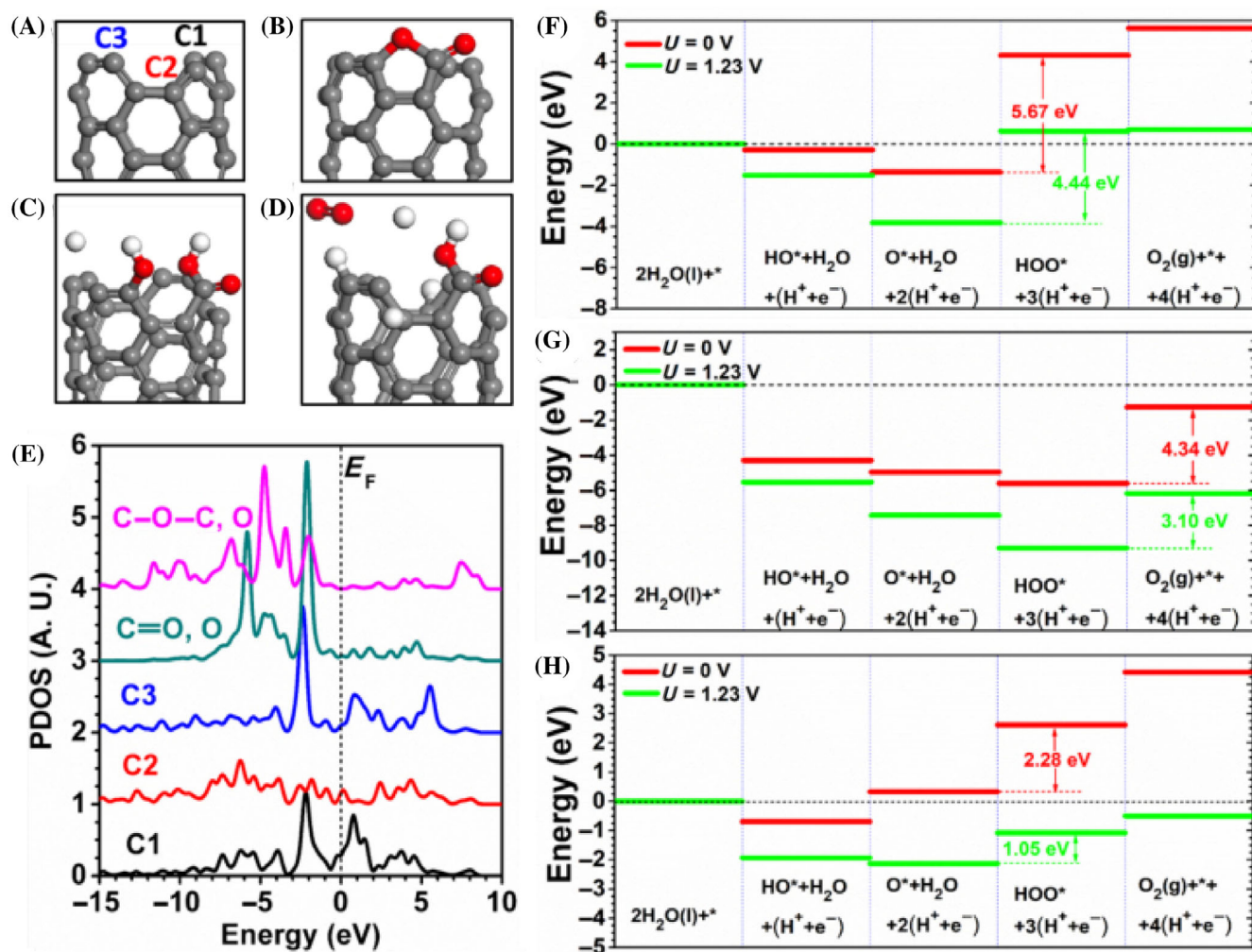
FIGURE 3 Geometric configurations and electronic properties of CNTs. (A) CNTs structure; (B, C) intermediates **3** and **4** in Scheme 1, respectively; (D) O_2 formation. (E) PDOS plots of CNTs with vacancies, oxidized CNTs and carboxylated CNTs. OER energy profiles for (F) CNTs with vacancies, (G) oxidized CNTs, and (H) carboxylated CNTs

reactivity. Hence, excellent OER performance can be expected on the highly active carboxyl modified surface of the CNTs.

In Figure 3F–H, the reactivities of the three different types of CNTs were compared in terms of the relative energies associated with the various steps of the OER process in Scheme 1. The energy diagram corresponding to CNTs with vacancies (Figure 3F) exhibits a downhill trend until epoxide **5** is formed, followed by a dramatic energy increase in the rate-determining step (RDS) of the process. This leads to the loss of OER activity of the CNTs due to a high energy barrier of 5.67 eV (Figure 3F). The energy diagram of the oxidized CNTs shows a similar uphill trend, with a slightly lower energy barrier of 4.34 eV for the deoxidization of peroxide **6** (Figure 3G). The lower barrier compared with that of the pure CNTs is consistent with the results of the polarization experiments. This energy barrier is attributed to the instability

of the oxidized groups during ambient geometry relaxation, and is thus dominated by the limited number of active sites on the CNTs surface. The reaction path for the carboxylated CNTs exhibits the same RDS as that observed for the untreated defective CNTs, that is, the reaction of epoxide **5** to peroxide **6** in Scheme 1. However, after the carboxylation of the CNTs, the stable carboxyl functional groups lead to a substantial decrease in the OER energy barrier to 2.28 eV (Figure 3H), which is less than half of that for the defective CNTs (Figure 3F). Further geometry optimizations show that all steps of the OER occur near the dangling [—C=O] bonds, which is consistent with the proposed Scheme 1. Notably, in the case of the carboxylated CNTs, most reaction steps in Scheme 1 are endothermic at zero overpotential, indicating that a positive overpotential is needed. Under a standard potential of 1.23 V, the maximum energy barrier for the carboxylated CNTs is further reduced to 1.05 eV
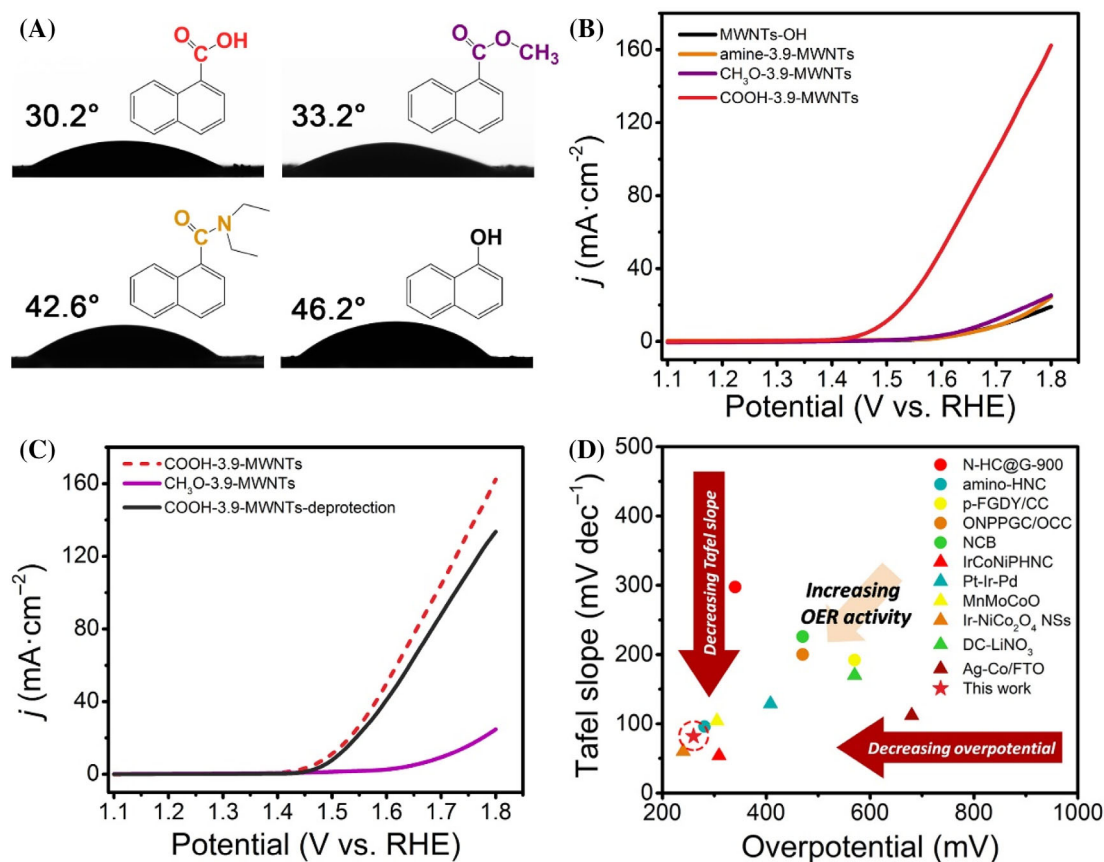
FIGURE 4 (A) Water contact angle of COOH-3.9-MWNTs, CH₃O-3.9-MWNTs, amine-3.9-MWNTs, and MWNTs-OH. (B) Polarization curves of the functionalized MWNTs. (C) Electrocatalytic properties of CH$_3$O-3.9-MWNTs and its deprotection. (D) Comparison of the acidic OER activity of the present MWNTs and other catalysts: Tafel slope versus η10 diagram

(Figure 3H). Therefore, the superior catalytic activity of the carboxylated CNTs in the OER process can be attributed to the presence of the active carboxyl groups, as shown in Scheme 1.

To further confirm the unique effect of the carboxyl groups on the OER performance of the MWNTs in acidic conditions, the COOH-3.9-MWNTs was functionalized with —OCH$_3$ and amine groups (designated as: CH$_3$O-3.9-MWNTs and amine-3.9-MWNTs) for protecting carboxyl and to investigate the effects of different groups on the OER process (Figure 4A; see Figures S25 and S26 for detailed structures). It is worth to note that esters and amides have a similar electronegativity[30] to the carboxylic acids incorporated in the CNTs, and they also have much better hydrophilicity than the pristine MWNTs (121.7°) and close to the COOH-3.9-MWNTs in 0.5 M H$_2$SO$_4$. However, their OER activities and ECSAs are considerably reduced compared with those of the COOH-3.9-MWNTs (Figures 4B and S27). In addition, MWNTs containing only hydroxyl groups (designated as: MWNTs-OH) was also investigated, which showed poor OER performance (Figure 4B), though a good hydrophilicity

(Figure 4A). These results suggest that carboxyl groups are responsible for the observed OER activity of COOH-3.9-MWNTs by enhancing not only the surface hydrophilicity, and hence the interaction with the electrolyte, but also the charge transfer to the reactants (Scheme 1). Interestingly, the catalytic performance of CH$_3$O-3.9-MWNTs could be almost fully recovered by hydrolyzation of CH$_3$O-3.9-MWNTs in alkaline solution (see Supporting Information) to recover the structure of COOH-3.9-MWNTs, as shown in Figure 4C. Once again, this clearly demonstrated the unique effect of carboxyl groups in enhancing the OER activity in acidic conditions.

As shown in Figure 4D, the newly-developed metal-free COOH-3.9-MWNTs exhibited outstanding OER performance in acidic conditions, outperformed most noble metal (e.g., Ir- and Ru)-based catalysts. To the best of our knowledge, they represent the best metal-free electrocatalysts for the acidic OER.[21–25,31–36] The methodology developed in this work could also be applied for the design and development of new carbon catalysts for OER and many other reactions.

3 | CONCLUSIONS

In summary, we have developed a class of highly efficient, stable, and low-cost acidic OER electrocatalyst based on metal-free carboxylic MWNTs, which show the best OER performance (a low overpotential of 265 mV at a current density of 10 mA cm^{-2} and a small Tafel slope of 82 mV dec^{-1}) among all metal-free electrocatalysts in acidic conditions reported to date, and comparable to those of RuO$_2$ and IrO$_2$ benchmark catalysts. Our experimental observations combined with the theoretical calculations revealed a novel OER mechanism for the carboxyl-enriched MWNTs, in which the carboxyl group lowers the energy barrier for water splitting via the formation and hydrolysis of a lactone. From a kinetic point of view, the introduction of carboxylic groups is beneficial for improving the hydrophilicity of the CNTs, and strengthening the interactions between catalyst and reactants. Thermodynamically, the carboxylic groups participate in the OER process via the formation and hydrolysis of a lactone, which lowers the energy barrier for the OER reaction. The methodology developed in this study is quite general, which can be used to design and develop new carbon catalysts for OER and other reactions important to high-performance water splitting, metal-air batteries and beyond.

4 | EXPERIMENTAL SECTION

4.1 | Chemicals

MWNTs prepared using Ni as the catalyst were purchased from Beijing Deke Daojin Science and Technology Co., Ltd. (China). All other chemicals were purchased from Sigma-Aldrich. Milli-Q-purified water with a resistance of 18.2 mΩ at 25°C was used throughout the study.

4.2 | Characterization

The morphologies of the composites were determined using scanning electron microscopy (SEM, Hitachi S-4800, Japan) and transmission electron microscopy (TEM, FEI Tecnai G2 F30, USA). X-ray photoelectron spectroscopy (XPS, ESCALAB 250xi, USA) was used to analyze the composition and valence states of the catalysts. The hydrophilicity of the materials was measured by a contact angle meter (DSA25, German Kruss). Raman spectra were recorded using a Hormonal HR800 Raman microscope with a 633 nm excitation source.

4.3 | Synthesis of o-MWNTs and COOH-3.9-MWNTs

The o-MWNTs were first prepared by dissolving 100 mg of MWNTs in piranha solution (10 ml of 98% H$_2$SO$_4$ and 3 ml of 30% H$_2$O$_2$) in a round-bottom flask (50 ml). The mixture was stirred gently at 22°C for different times: 10, 15, 20, 25, and 30 h. The corresponding o-MWNTs were then collected by centrifugal separation, washed thoroughly with water and ethanol until the pH became neutral, and then dried under vacuum overnight.

The as-obtained o-MWNTs were further treated through a simple hydrothermal reaction, by adding 15 ml of ultrapure water with intense sonication for approximately 1 h. The o-MWNTs were then transferred into a Teflon-lined autoclave and reacted at 180°C for 12 h. The COOH-3.9-MWNTs products were then collected by repeated centrifugation and washing with water and ethanol, followed by drying under vacuum overnight. The compared samples were synthesized with the similar processes by changing hydrothermal temperature and reaction time.

4.4 | Synthesis of Ni/MWNTs

Ni/MWNTs samples were synthesized through a facile hydrothermal method as follows: 27.4 mg of Ni(NO$_3$)$_2$·6H$_2$O was dissolved in glycol and sonicated for approximately 30 min. Subsequently, 4 ml of sodium hydroxide (1 M) solution and 10 mg of MWNTs were added to the above mixture with vigorous stirring for approximately 1 h. The as-obtained suspension was transferred into a Teflon-lined autoclave and reacted at 110°C for 4 h. Finally, the resulting product was filtered, washed, dispersed in ethanol, and then dried under vacuum overnight.

4.5 | Synthesis of methyl benzoate and esterification of MWNTs (CH$_3$O-3.9-MWNTs)

A 1.22 g (0.01 mol) amount of benzoic acid was dissolved in 50 ml methanol in a 100 ml round-bottom flask. Then, 2 ml concentrated sulfuric acid (98%) was added dropwise to the solution in an ice bath, with vigorous stirring for 5 min. After that, the mixture was transferred into an oil bath and refluxed for 3 h. After cooling, the excess methanol was evaporated under vacuum. The remaining liquid was partitioned with water/ethyl acetate (EtOAc), washed with water until neutral pH, and dried over MgSO$_4$; then, the solvent was removed to yield a

colorless oil. ^{1}H NMR (400 MHz, CDCl$_3$) $\delta = 8.04$ (d, $J = 7.1$ Hz, 2H), 7.54 (t, $J = 7.4$ Hz, 1H), 7.43 (t, $J = 7.6$ Hz, 2H), 3.91 (s, 3H). ^{13}C NMR (100 MHz, CDCl$_3$) $\delta = 167.2, 133.0, 130.2, 129.7, 128.4, 52.2$; IR (KBr): 2960, 2918, 2867, 1616, 1415, 1359, 1273, 1206, 1079, 770 cm^{-1}.

COOH-3.9-MWNTs were functionalized with CH$_3$O group (designated as: CH$_3$O-3.9-MWNTs). The CH$_3$O-3.9-MWNTs samples were synthesized by a similar method. After stirring for 3 h, the mixture was washed with deionized water until neutral pH and dried under vacuum.

4.6 | Deprotection of CH$_3$O-3.9-MWNTs

Fifty milligrams of CH$_3$O-3.9-MWNTs was stirred in 25 ml 1.0 M NaOH solution under 60°C for 5 h in a 100 ml round-bottom flask. Then the pH was adjusted to 1 by dropwise adding HCl. After stirring for another 5 h, the deprotection MWNTs (COOH-3.9-MWNTs-deprotection) was obtained by centrifugation with deionized water until neutral pH and dried under vacuum.

4.7 | Synthesis of *N,N*-diethylbenzamide

After dissolving 5.8 ml (0.056 mol) diethylamine in 10 ml anhydrous tetrahydrofuran (THF) in a 100 ml round-bottom flask, 1.67 (0.07 mol) NaH was introduced in the solution with vigorous stirring for 30 min. Then, 5 ml benzoyl chloride was dissolved in 10 ml anhydrous THF and the as-prepared solution was added dropwise to the above mixture with stirring for 1 h at room temperature. After that, the solvent was evaporated and the residue was partitioned with water/EtOAc. Then, the organic layer was dried over MgSO$_4$ and the solvent was removed to yield a colorless oil. ^{1}H NMR (400 MHz, CDCl$_3$) δ 7.31 (m, 5H), 3.48 (m, 2H), 3.19 (m, 2H), 1.18 (m, 3H), 1.04 (m, 3H). ^{13}C NMR (100 MHz, CDCl$_3$) δ 171.2, 137.2, 129.0, 128.3, 126.2, 43.2, 39.2, 14.1, 12.8; IR (KBr): 3068, 3000, 2953, 1729, 1600, 1450, 1276, 1176, 1107, 1065 cm^{-1}.

4.8 | Synthesis of amide-functionalized MWNTs (amine-3.9-MWNTs)

COOH-3.9-MWNTs were functionalized with amine group (designated as: amine-3.9-MWNTs). In a 50 ml round-bottom flask, 10 mg COOH-3.9-MWNTs was mixed with 2 ml thionyl chloride (SOCl$_2$) and 50 µl DMF under vigorous stirring and refluxed for 6 h. The excess SOCl$_2$ was then removed to obtain MWNTs functionalized with acyl chloride. The amine-3.9-MWNTs were obtained by replacing benzoyl chloride in the above MWNTs functionalized with acyl chloride. After stirring for 1 h, the mixture was washed with deionized water until neutral pH and dried under vacuum.

4.9 | Electrochemical measurements

After dispersing 4 mg of the treated COOH-3.9-MWNTs in *N,N*-dimethylformamide (DMF, 1 ml) solution, 20 µl of 5 wt% Nafion was added to the mixture, followed by sonication for 30 min to form a homogeneous ink. Twenty microliters of the COOH-3.9-MWNT ink were used to modify the surface of a glassy carbon electrode (GCE) and dried in a bulb. All electrochemical measurements were carried out on a CHI 760E electrochemical workstation (CH instruments, Shanghai Chenhua Instrument Corp., China) with a typical three-electrode configuration consisting of a GCE modified with the COOH-3.9-MWNT catalyst, a Pt auxiliary electrode, and an Ag/AgCl reference electrode with 0.5 M H$_2$SO$_4$ or 0.1 M HClO$_4$ solution as the electrolyte. Polarization curves were recorded using linear potential sweeps at a typical scan rate of 10 mV s^{-1}. All rotating ring-disk electrode (RRDE) voltammograms were recorded at a rotating rate of 1600 rpm. The reported potentials are referenced to the RHE, by converting the obtained potentials (vs. Ag/AgCl) to the RHE scale using the following equation: $E_{vs.\ RHE} = E_{vs.\ Ag/AgCl} + 0.198$ V $+ 0.059$ pH. Electrochemical impedance spectroscopy (EIS) measurements were performed in an electrolyte solution of 0.5 M H$_2$SO$_4$, with a frequency range from 0.1 to 10^5 Hz and an AC probe amplitude of 400 mV. The Mott–Schottky curves were collected from 0.4 to 0.9 V versus RHE at the frequency of 1000 Hz in Ar-saturated 0.5 M H$_2$SO$_4$. The produced O$_2$ via OER process was quantified by gas chromatography (GC, 7890B, Ar carrier, Agilent).

4.10 | RRDE measurements

The oxygen generated and detected on the disk electrode during the anodic polarization scan was reduced on the Pt ring electrode at a constant potential of 0.4 V versus RHE by the oxygen reduction reaction (ORR). The collection efficiency (N) of the RRDE was determined to be 37%.[28] During the Faradaic efficiency measurements, the glassy carbon disk potential was set at 1.4 V versus RHE to enable the OER to proceed: $2H_2O \rightarrow O_2 + 4H^+ + 4e^-$. The generated oxygen was detected on the Pt ring disk through the ORR process. The Faraday efficiency was calculated using the following equation: $FE = \frac{j_{ORR}}{j_{OER} \times N} \times 100\%$,

where j_{ORR} and j_{OER} are the stabilized current densities obtained on the Pt ring and glassy carbon disk, respectively. The H_2O_2 detection was also performed by applying the ring potential of 1.5 V versus RHE on RRDE.

4.11 | Calculation of electrochemically active surface areas

The ECSA of the COOH-3.9-MWNT electrodes was estimated from the electrochemical double-layer capacitance (C_{dl}) of the catalytic surface. The latter was determined from the scan rate dependence of CVs carried out in a potential range of 0.9–1.2 V versus RHE, where no Faradaic current is present, at various scan rates (20–120 mV s^{-1}). In particular, C_{dl} was obtained as half the slope of a plot of the current density (j) difference between anodic and cathodic sweeps ($j_{anodic} - j_{cathodic}$) at 0.1 V versus RHE against the scan rate. Then, the ECSA value was calculated from C_{dl} according to the following equation:

$$ECSA = \frac{C_{dl} \, (mF \, cm^{-2})}{40 \, \mu F \, cm^{-2} \, per \, cm^2_{ECSA}},$$

where the denominator represents the specific capacitance value for a flat standard with 1 cm^2 of real surface area.

CONFLICT OF INTEREST
The authors declare no conflict of interest.

ORCID
Fengchun Yang 🄳 https://orcid.org/0000-0002-0863-6404

REFERENCES
1. Suen NT, Hung SF, Quan Q, Zhang N, Xu YJ, Chen HM. Electrocatalysis for the oxygen evolution reaction: recent development and future perspectives. *Chem Soc Rev*. 2017;45(2):337-365.
2. Hunter BM, Gray HB, Müller AM. Earth-abundant heterogeneous water oxidation catalysts. *Chem Rev*. 2016;116(22):14120-14136.
3. Reier T, Nong HN, Teschner D, Schlögl R, Strasser P. Electrocatalytic oxygen evolution reaction in acidic environments—reaction mechanisms and catalysts. *Adv Energy Mater*. 2016;7:1601275.
4. Seitz LC, Dickens CF, Nishio K, et al. A highly active and stable IrO$_x$/SrIrO$_3$ catalyst for the oxygen evolution reaction. *Science*. 2016;353(6303):1011-1014.
5. Frydendal R, Paoli EA, Chorkendorff I, Rossmeisl J, Stephens IEL. Toward an active and stable catalyst for oxygen evolution in acidic media: Ti-stabilized MnO$_2$. *Adv Energy Mater*. 2015;5:1500991.
6. McCrory CCL, Jung S, Peters JC, Jaramillo TF. Bench-marking heterogeneous electrocatalysts for the oxygen evolution reaction. *J Am Chem Soc*. 2013;135(45):16977-16987.
7. Kim J, Shih PC, Tsao KC, et al. High-performance pyrochlore-type yttrium ruthenate electrocatalyst for oxygen evolution reaction in acidic media. *J Am Chem Soc*. 2017;139(34):12076-12083.
8. Reier T, Pawolek Z, Cherevko S, et al. Molecular insight in structure and activity of highly efficient, low-Ir Ir–Ni oxide catalysts for electrochemical water splitting (OER). *J Am Chem Soc*. 2015;137(40):13031-13040.
9. Lei C, Chen H, Cao J, et al. Fe–N$_4$ sites embedded into carbon nanofiber integrated with electrochemically exfoliated graphene for oxygen evolution in acidic medium. *Adv Energy Mater*. 2018;8:1801912.
10. Qu KG, Zheng Y, Jiao Y, Zhang X, Dai S, Qiao SZ. Polydopamine-inspired, dual heteroatom-doped carbon nanotubes for highly efficient overall water splitting. *Adv Energy Mater*. 2017;7:1602068.
11. Ma T, Dai S, Jaroniec M, Qiao SZ. Graphitic carbon nitride nanosheet-carbon nanotube three-dimensional porous composites as high-performance oxygen evolution electrocatalysts. *Angew Chem Int Ed*. 2014;53(28):7281-7285.
12. Mo C, Jian J, Li J, et al. Boosting water oxidation on metal-free carbon nanotubes via directional interfacial charge-transfer induced by an adsorbed polyelectrolyte. *Energy Environ Sci*. 2018;11(12):3334-3341.
13. Hu C, Dai L. Doping of carbon materials for metal-free electrocatalysis. *Adv Mater*. 2019;31:1804672.
14. Hu C, Dai L. Carbon-based metal-free catalysts for electrocatalysis beyond the ORR. *Angew Chem Int Ed*. 2016;55(39):11736-11758.
15. Zhu J, Kim J, Peng H, Margrave JL, Khabashesku VN, Barrera EV. Improving the dispersion and integration of single-walled carbon nanotubes in epoxy composites through functionalization. *Nano Lett*. 2003;3(8):1107-1113.
16. Hsieh CT, Chen WY, Cheng YS. Influence of oxidation level on capacitance of electrochemical capacitors fabricated with carbon nanotube/carbon paper composites. *Electrochim Acta*. 2010;55(19):5294-5300.
17. Zhang W, Zhang X, Chen L, et al. Single-walled carbon nanotube induced optimized electron polarization of rhodium nanocrystals to develop an interface catalyst for highly efficient electrocatalysis. *ACS Catal*. 2018;8(9):8092-8099.
18. Meyer AG, Dai L, Chen Q, Easton CJ, Xia L. Selective adsorption of nitro-substituted aromatics and accelerated hydrolysis of 4-nitrophenyl acetate on carbon surfaces. *New J Chem*. 2001;25(7):887-889.
19. Jeon IY, Choi HJ, Jung SM, et al. Large-scale production of edge-selectively functionalized graphene nanoplatelets via ball milling and their use as metal-free electrocatalysts for oxygen reduction reaction. *J Am Chem Soc*. 2013;135(4):1386-1393.

20. Lin YX, Feng WJ, Zhang JJ, et al. A polyimide nanolayer as a metal-free and durable organic electrode toward highly efficient oxygen evolution. *Angew Chem Int Ed*. 2018;57(38):12563-12566.

21. Sun J, Lowe SE, Zhang L, et al. Ultrathin nitrogen-doped holey carbon@graphene bifunctional electrocatalyst for oxygen reduction and evolution reactions in alkaline and acidic media. *Angew Chem Int Ed*. 2018;57(50):16511-16515.

22. Zhao X, Su H, Cheng W, et al. Operando insight into the oxygen evolution kinetics on the metal-free carbon-based electrocatalyst in an acidic solution. *ACS Appl Mater Interfaces*. 2019;11(38):34854-34861.

23. Xing C, Xue Y, Huang B, et al. Fluorographdiyne: a metal-free catalyst for applications in water reduction and oxidation. *Angew Chem Int Ed*. 2019;58(39):13897-13903.

24. Lai J, Li S, Wu F, Saqib M, Luque R, Xu G. Unprecedented metal-free 3D porous carbonaceous electrodes for full water splitting. *Energy Environ Sci*. 2016;9(4):1210-1214.

25. Zhu Y, Zhang T, Lee JY. Nitrogenated-graphite-encapsulated carbon black as a metal-free electrocatalyst for the oxygen evolution reaction in acid. *ChemElectroChem*. 2018;5(4):583-588.

26. Chen S, Duan J, Jaroniec M, Qiao SZ. Nitrogen and oxygen dual-doped carbon hydrogel film as a substrate-free electrode for highly efficient oxygen evolution reaction. *Adv Mater*. 2014;26(18):2925-2930.

27. Zhang Y, Fan X, Jian J, Yu D, Zhang Z, Dai L. A general polymer-assisted strategy enables unexpected efficient metal-free oxygen-evolution catalysis on pure carbon nanotubes. *Energy Environ Sci*. 2017;10(11):2312-2317.

28. Chen P, Xu K, Zhou T, et al. Strong-couple cobalt borate nanosheets/graphene hybrid as electrocatalyst for water oxidation under both alkaline and neutral conditions. *Angew Chem Int Ed*. 2016;55(7):2488-2492.

29. Liu R, Wang Y, Liu D, Zou Y, Wang S. Water-plasma-enabled exfoliation of ultrathin layered double hydroxide nanosheets with multivacancies for water oxidation. *Adv Mater*. 2017;29:1701546.

30. Hansch C, Leo A, Taft RW. A survey of Hammett substituent constants and resonance and field parameters. *Chem Rev*. 1991;91(2):165-195.

31. Feng J, Lv F, Zhang W, et al. Iridium-based multimetallic porous hollow nanocrystals for efficient overall-water-splitting catalysis. *Adv Mater*. 2017;29:1703798.

32. Zhu J, Xie M, Chen Z, et al. Pt–Ir–Pd trimetallic nanocages as a dual catalyst for efficient oxygen reduction and evolution reactions in acidic media. *Adv Energy Mater*. 2020;10:1904114.

33. Delgado D, Minakshi M, McGinnity J, Kim DJ. Co/Mo bimetallic addition to electrolytic manganese dioxide for oxygen generation in acid medium. *Sci Rep*. 2015;5:15208.

34. Yin J, Jin J, Lu M, et al. Iridium single atoms coupling with oxygen vacancies boosts oxygen evolution reaction in acid media. *J Am Chem Soc*. 2020;142(43):18378-18386.

35. Yang S, Zhan Y, Yang L, Lee JY. Dichotomizing the oxygen electrocatalytic properties of doped carbon catalysts in acid through a salt-activated synthesis. *ChemCatChem*. 2017;9(1):103-108.

36. Yan KL, Chi JQ, Xie JY, et al. Mesoporous Ag-doped Co_3O_4 nanowire arrays supported on FTO as efficient electrocatalysts for oxygen evolution reaction in acidic media. *Renew Energy*. 2018;119(1):54-61.

SUPPORTING INFORMATION

Additional supporting information may be found in the online version of the article at the publisher's website.